

2D nanoporous membrane for cation removal from water: effects of ionic valence, membrane hydrophobicity and pore size

Mateus Henrique Köhler,^{1, a)} José Rafael Bordin,^{2, b)} and Marcia C. Barbosa¹

¹⁾*Instituto de Física, Universidade Federal do Rio Grande do Sul,
Caixa Postal 15051, 91501-970, Porto Alegre, Brazil*

²⁾*Campus Caçapava do Sul, Universidade Federal do Pampa,
Av. Pedro Anunciação 111, CEP 96570-000, Caçapava do Sul,
Brazil*

Using molecular dynamic simulations we show that single-layers of molybdenum disulfide (MoS_2) and graphene can effectively reject ions and allow high water permeability. Solutions of water and three cations with different valence (Na^+ , Zn^{2+} and Fe^{3+}) were investigated in the presence of the two types of membranes and the results indicate a high dependence of the ion rejection on the cation charge. The associative characteristic of ferric chloride leads to a high rate of ion rejection by both nanopores, while the monovalent sodium chloride induces lower rejection rates. Particularly, MoS_2 shows 100% of Fe^{3+} rejection for all pore sizes and applied pressures. On the other hand, the water permeation did not varies with the cation valence, having dependence only with the nanopore geometric and chemical characteristic. This study helps to understand the fluid transport through nanoporous membrane, essential for the development of new technologies for pollutants removal from water.

Keywords: heavy metals, water purification, nanopores, molybdenum disulfide, graphene

^{a)}Electronic mail: mateus.kohler@ufrgs.br

^{b)}Electronic mail: josebordin@unipampa.edu.br

I. INTRODUCTION

Centuries of misuse of natural resources has stressed available freshwater supplies throughout the world. With the rapid development of industries, chemical waste has been thrown deliberately in water to the point of making it difficult to clean. Particularly, direct or indirect discharge of heavy metals into the environment has increased recently, especially in developing countries¹. Unlike organic contaminants, heavy metals are not biodegradable and tend to accumulate in living organisms. Many heavy metal ions are known also to be toxic or carcinogenic². Toxic heavy metals of particular concern in treatment of industrial waste-water include zinc, copper, iron, mercury, cadmium, lead and chromium.

As a result, filtration process that can acquire freshwater from contaminated, brackish water or seawater is an effective method to also increase the potable water supply. Modern desalination is mainly based on reverse osmosis (RO) performed through membranes, due to their low energy consumption and easy operation. Current RO plants have already operated near the thermodynamic limit, with the applied pressure being only 10 to 20% higher than the osmotic pressure of the concentrate³. Meanwhile, advances in nanotechnology have inspired the design of novel membranes based on two-dimensional (2D) nanomaterials. Nanopores with diameters ranging from a few Angstroms to several nanometers can be drilled in membranes to fabricate molecular sieves⁴. As the diameter of the pore approaches the size of the hydrated ions, various types of ions can be rejected by nanoporous membranes leading to efficient water desalination. Graphene, a single-atom-thick carbon membrane was demonstrated to have several orders of magnitude higher flux rates when compared with conventional zeolite membranes⁵. In this way, graphene and graphene oxidized are one of the most prominent materials for high-efficient membranes⁶⁻⁸. More recently, others 2D materials have also been investigated for water filtration. A nanoporous single-layer of molybdenum disulfide (MoS_2) has shown great desalination capacity⁹⁻¹¹. The possibility to craft the pore edge with Mo, S or both provides flexibility to design the nanopore with desired functionality. In the same way, boron nitride nanosheets also has been investigated for water purification from distinct pollutants^{12,13}. Therefore, not only the nanopore size matters for cleaning of water purposes but also the hydrophobicity and geometry of the porous.

For instance, the performance of commercial RO membrane is usually on the order of 0.1 $\text{L}/\text{cm}^2 \cdot \text{day} \cdot \text{MPa}$ ($1.18 \text{ g}/\text{m}^2 \cdot \text{s} \cdot \text{atm}$)¹⁴. With the aid of zeolite nanosheets, permeability high

as $1.3 \text{ L/cm}^2 \cdot \text{day} \cdot \text{MPa}$ can be obtained¹⁵. Recent studies has show that MoS_2 nanopore filters have potential to achieve a water permeability of roughly $100 \text{ g/m}^2 \cdot \text{s} \cdot \text{atm}^{10}$ – 2 orders of magnitude higher than the commercial RO. This is comparable with that measured experimentally for the graphene filter ($\sim 70 \text{ g/m}^2 \cdot \text{s} \cdot \text{atm}$) under similar conditions¹⁶. These results have shown that the water permeability scales linearly with the pore density. Therefore, the water filtering performance of 2D nanopores can be even higher.

Controlling the size and shape of the pores created in these membranes, however, represents a huge experimental challenge. Inspired by a number of molecular dynamics studies predicting ultrahigh water permeability across graphene and others 2D nanoporous membranes^{11,17}, technologies have been developed to either create and control the nanopore size and distribution. Methods including electron beam¹⁸, ion irradiation¹⁹ and chemical etching²⁰ have been reported to introduce pores in graphene. J. Feng et al.²¹ have also developed a scalable method to controllably make nanopores in single-layer MoS_2 with subnanometer precision using electrochemical reaction (ECR). Recently, K. Liu and colleagues²² investigated the geometrical effect of the nanopore shape on ionic blockage induced by DNA translocation through h-BN and MoS_2 nanopores. They observed a geometry-dependent ion scattering effect, and further proposed a modified ionic blockage model which is highly related to the ionic profile caused by geometrical variations. Additionally, recent experimental efforts have been devoted to amplify the filtering efficiency of the nanoporous membranes. Z. Wang and colleagues²³ mechanistically related the performance of MoS_2 membranes to the size of their nanochannels in different hydration states. They attributed the high water flux ($30\text{-}250 \text{ L/m}^2 \cdot \text{h} \cdot \text{bar}$) of MoS_2 membranes to the low hydraulic resistance of the smooth, rigid MoS_2 nanochannels. The membrane compaction with high pressure have also been found to create a neatly stacked nanostructure with minimum voids, leading to stable water flux and enhanced separation performance. By tuning the pore creation process, D. Jang et al.²⁴ have demonstrated nanofiltration membranes that reject small molecules but offer high permeance to water or monovalent ions. Also, studies have shown how defects, oxidation and functionalization can affect the ionic blockage²⁵⁻²⁷ All of these studies point to a near future where 2D membranes will have a major impact on desalination processes.

In this work, we address the issue of the selectivity of the porous. In order to do that, we compare the water filtration capacity of MoS_2 and graphene through molecular dynamics simulations. While graphene is a purely hydrophobic material, MoS_2 sheets have both

hydrophobic (S) and hydrophilic (Mo) sites. Recent studies have shown that the water dynamics and structure inside hydrophobic or hydrophilic pores can be quite distinct regarding the pore size²⁸⁻³⁰ and even near hydrophobic or hydrophilic protein sites³¹. Three cations are considered: the standard monovalent sodium (Na^+), the divalent zinc (Zn^{2+}) and trivalent iron (Fe^{3+}). The study of sodium removal is relevant due to its applications for water desalination³²⁻³⁴. Zinc is a trace element that is essential for human health. It is important for the physiological functions of living tissue and regulates many biochemical processes. However, excess of zinc can cause eminent health problems³⁵. The cation Zn^{2+} is ranked 75th in the *Comprehensive Environmental Response, Compensation and Liability Act* (CERCLA) 2017 priority list of hazardous substances. In its trivalent form, ferric chloride $\text{Fe}^{3+}\text{Cl}_3^-$ is a natural flocculant, with high power of aggregation. It is also on the CERCLA list with recommended limit concentration of 0.3 mg/l. In this way, we explore the water permeation and cations rejection by nanopore with distinct radii. Our results show that the hydrophilic/hydrophobic MoS_2 nanopore have a higher salt rejection in all scenarios, while the purely hydrophobic graphene have a higher water permeation. Specially, MoS_2 membranes show the impressive capacity of block all the trivalent iron cations regardless the nanopore size.

Our paper is organized as follows. In Section II we introduce our model and the details about the simulation method. In Section III we show and discuss our results for the water permeation in the distinct membranes, while in Section IV we show the ion rejection properties for each case. Finally, a summary of our results and the conclusions are shown in Section V.

II. COMPUTATIONAL DETAILS AND METHODS

Molecular dynamics (MD) simulations were performed using the LAMMPS package³⁶. A typical simulation box consists of a graphene sheet acting as a rigid piston in order to apply an external force (pressure) over the ionic solution. The pressure gradient forces the solution against the 2D nanopore: a single-layer of molybdenum disulfide or graphene. Figure 1 shows the schematic representation of the simulation framework.

A nanopore was drilled in both MoS_2 and graphene sheets by removing the desired atoms, as shown in Figure 1. The accessible pore diameters considered in this work range from 0.26

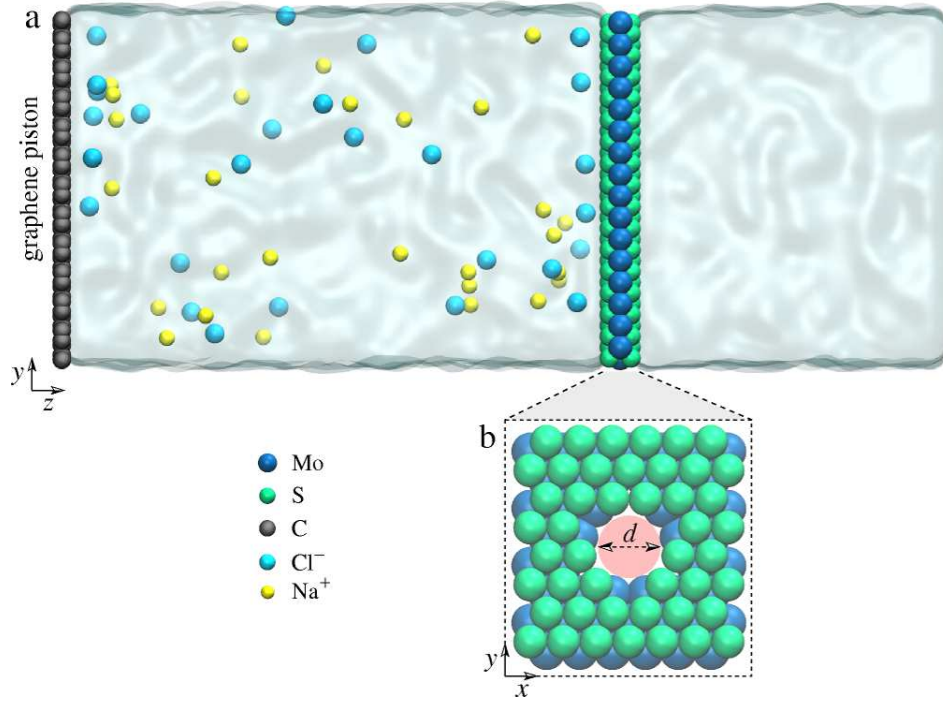


FIG. 1. (a) Schematic representation of the simulation framework. The system is divided as follows: On the left side we can see the piston (graphene) pressing the ionic solution (in this case, water+NaCl) against the MoS₂ nanopore. For the case of a graphene nanopore the depiction is the same, but with a porous graphene sheet instead of the MoS₂ sheet. On the right side we have bulk water. (b) Definition of the pore diameter d .

- 0.95 nm for the MoS₂ (which means a pore area ranging from 5.5 - 71 Å²) and 0.17 - 0.92 nm for the graphene (with area ranging from 2.5 - 67 Å²). M. Heiranian et al.¹¹ have studied different MoS₂ nanopore's composition for water filtration: with only Mo, only S and a mix of the two atoms at the pore's edge. They found similar ion rejection rates for both cases. Here, in order to account for circular nanopores, mixed pore edges have been chosen. The system contains 22000 atoms distributed in a box with dimensions 5 × 5 × 13 nm in x, y and z, respectively. Although the usual salinity of seawater is ~ 0.6M, we choose a molarity of ~ 1.0M for all the cations (Na⁺, Zn²⁺ and Fe³⁺) due the computational cost associated with low-molarity solutions.

The TIP4P/2005³⁷ water model was used and the SHAKE algorithm³⁸ was employed to maintain the rigidity of the water molecules. The non-bonded interactions are described by the Lennard-Jones (LJ) potential with a cutoff distance of 0.1 nm and the parameters tabu-

TABLE I. The Lennard-Jones parameters and charges of the simulated atoms. The crossed parameters were obtained by Lorentz-Berthelot rule.

Interaction	σ (nm)	ε (kcal/mol)	Charge
C–C ⁴⁰	3.39	0.0692	0.00
Mo–Mo ⁴¹	4.20	0.0135	0.60
S–S ⁴¹	3.13	0.4612	-0.30
O–O ³⁷	3.1589	0.1852	-1.1128
H–H	0.00	0.00	0.5564
Na–Na ⁴²	2.52	0.0347	1.00
Cl–Cl ⁴²	3.85	0.3824	-1.00
Zn–Zn ⁴³	0.0125	1.960	2.00
Fe–Fe ⁴³	0.18	0.745	3.00

lated in Table 1. The Lorentz-Berthelot mixing rule were used to obtain the LJ parameters for different atomic species. The long-range electrostatic interactions were calculated by the *Particle Particle Particle Mesh* method³⁹. Periodic boundary conditions were applied in all the three directions.

For each simulation, the system was first equilibrated for constant number of particles, pressure and temperature (NPT) ensemble for 1 ns at $P = 1$ atm and $T = 300$ K. Graphene and MoS₂ atoms were held fixed in the space during equilibration and the NPT simulations allow water to reach its equilibrium density (1 g/cm³). After the pressure equilibration, a 5 ns simulation in the constant number of particles, volume and temperature (NVT) ensemble to further equilibrate the system at the same $T = 300$ K. Finally, a 10 ns production run were carried out, also in the NVT ensemble. The Nosé-Hoover thermostat^{44,45} was used at each 0.1 ps in both NPT and NVT simulations, and the Nosé-Hoover barostat was used to keep the pressure constant in the NPT simulations. Different external pressures were applied on the rigid piston to characterize the water filtration through the 2D (graphene and MoS₂) nanopores. For simplicity, the pores were held fixed in space to study solely the water

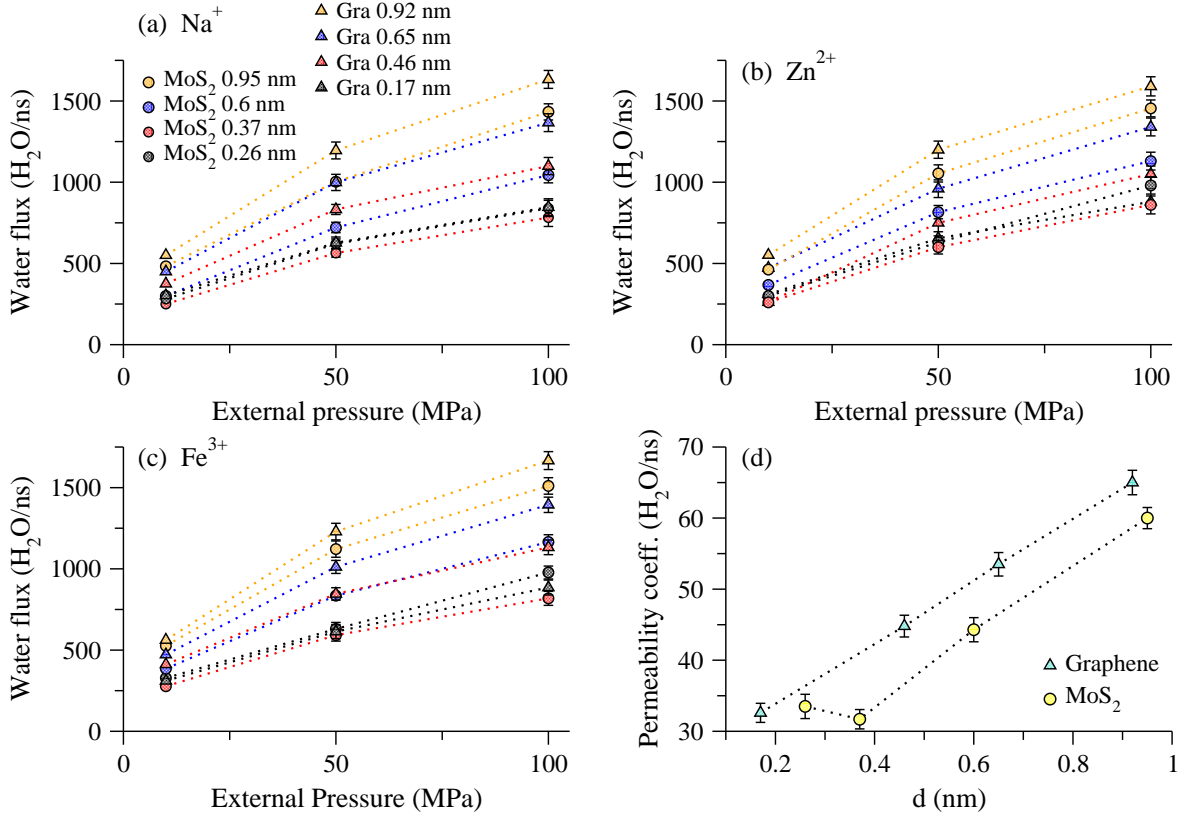


FIG. 2. Water flux as a function of the applied pressure for MoS₂ and graphene nanopores with similar pore areas. (a) monovalent Na⁺, (b) divalent Zn²⁺ and (c) trivalent Fe³⁺ cations are considered for the ionic solution at the reservoir. (d) Water permeability through the pores as function of the pore diameter for the case of $\Delta P = 50$ MPa. The dotted lines are a guide to the eye.

transport and ion rejection properties of these materials. The external pressures range from 10 to 100 MPa. These are higher than the osmotic pressure used in the experiments. The reason for applying such high pressures at MD simulations with running time in nanosecond scale is because the low pressures would yield a very low water flux that would not go above the statistical error. We carried out three independent simulations for each system collecting the trajectories of atoms every picoseconds.

III. WATER FLUX

First, let us compare the flux performance of the graphene and the MoS₂ membranes. In the Figure 2, we show the water flux through 2D nanopores in number of molecules per nanosecond (MoS₂ and graphene) as a function of the applied pressure gradient for different pore diameters. The water is filtered from a reservoir containing an ionic solution of either monovalent sodium (Na⁺), divalent zinc (Zn²⁺) or trivalent iron cations (Fe³⁺). In all cases, chlorine (Cl⁻) was used as the standard anion. Four pore sizes for each material were investigated.

Our results indicates that for the smaller pore diameter, the black points in the Figure 2, both materials have the same water permeation. However, for the other values of pore diameter the graphene membrane shows a higher water flux, for all applied pressure gradient. While the flux at the purely hydrophobic graphene pore for a fixed pressure monotonically increases with the pore diameter, this is not the case for the MoS₂ pore for which the flows shows a minimum around pore diameter of 0.37 nm probably due to the non uniform distribution of the hydrophobic and hydrophilic sites of the pore. The Figures 2(a), (b) and (c) show that this behavior of the water flux is not affected by the cation valence, only by the applied pressure, by geometric effects and by the pore composition. For instance, the 0.46 nm graphene pore shows enhanced water flux compatible with the 0.6 nm MoS₂ pore for all cations. Therefore, is clear that pore composition affects the water permeation properties more than the water-ion interaction.

This result agrees with the findings by Aluru and his group¹¹, were they showed that even a small change in pore composition can lead to enhanced water flux through a MoS₂ nanocavity. This is also consistent with our recent findings that the dynamics of water inside nanopores with diameter ≈ 1.0 nm is strongly affected by the presence of hydrophilic or hydrophobic sites²⁹. This investigation, over distinct cation valences and membranes, highlights the importance of the nanopore physical-chemistry properties for water filtration processes.

To quantify the water permeability through the pores, we compute the permeability coefficient, p , across the pore. For dilute solutions

$$p = \frac{j_w}{-V_w \Delta C_s + \frac{V_w}{N_A k_B T} \Delta P} \quad (1)$$

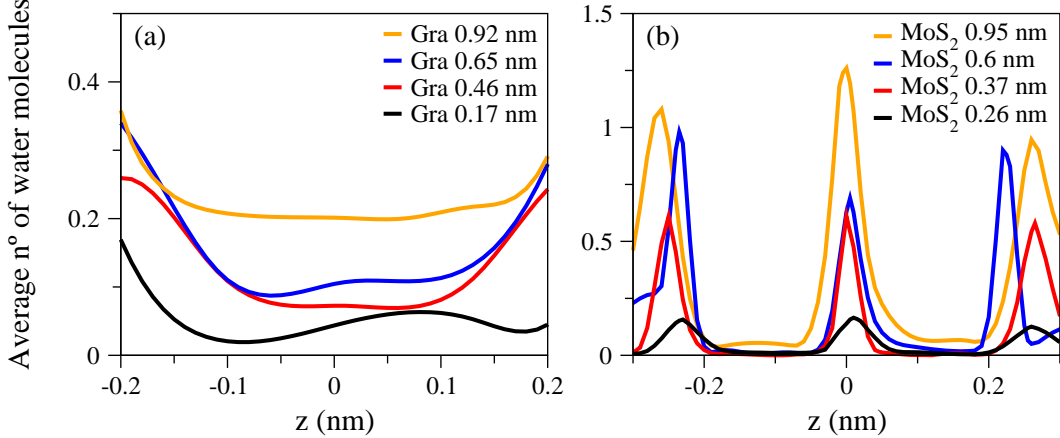


FIG. 3. Averaged axial distribution of water molecules inside the (a) graphene (Gra) and (b) MoS₂ nanopores with distinct diameters. Here, $z = 0$ is at the center of the pore, the external pressure is $\Delta P = 10$ MPa and the cation is the Na⁺.

where j_w is the flux of water (H₂O/ns), V_w is the molar volume of water (19 ml/mol), ΔC_s is the concentration gradient of the solute (1.0 M), N_A is the Avogadro number, k_B is the Boltzmann constant, T is the temperature (300 K) and ΔP is the applied hydrodynamic pressure (MPa).

The case of $\Delta P = 50$ MPa is shown in Figure 2(d). The permeability coefficient of the MoS₂ range from approximately 33 to 55 H₂O/ns for the 0.26 and 0.95 nm diameters, respectively. The graphene nanopore presents a permeability coefficient of $\sim 34 - 63$ H₂O/ns as the pore diameter is varied from 0.17 to 0.92 nm, respectively. For smaller pores the difference between MoS₂ and graphene is inside the error bars, whereas for the larger pores both materials exhibit high permeability rates, with a slight advantage in the case of graphene.

The water structure and dynamics inside nanopores are strongly related^{29,46}. Therefore, distinct structural regimes can lead to different diffusive behaviors. In the Figure 3 we present the distribution of water molecules in the z -direction inside the MoS₂ (solid line) and graphene (dotted line) nanopores. As for the water flux, the water axial distribution is not affected by the cation valence. Therefore, for simplicity and since there are more studies about monovalent salts, we show only the Na⁺ case. The nanopore length in the z -direction, considering the van der Waals diameter for each sheet, is 0.63 (-0.315 to 0.315) nm for the MoS₂ and 0.34 (-0.17 to 0.17) nm for the graphene. The structure inside both pores are considerably different. For the graphene nanopore, shown in Figure 3(a), there is

no favorable positions for the water molecules to remain throughout the simulation. This can be related to the hydrophobic characteristic of the graphene sheet and the high slippage observed for water inside carbon nanopores^{47,48}. Since all the pore is hydrophobic, there is no preferable position for the water molecules, and the permeability is higher. On the other hand, along the MoS₂ cavity we can observe a high structuration in three sharp peaks, as shown in Figure 3(b). This structuration comes from the existence of hydrophilic (Mo) and hydrophobic sites (S atoms). This layered organization within the MoS₂ nanopore can be linked to the reduced flux compared with graphene, since it implies an additional term in the energy required for the water molecule to pass through the pore.

The higher water flux through graphene nanopores compared with MoS₂ imply that for a desired water flux, a smaller applied pressure is needed for graphene. Nevertheless, it is important to note that both fluxes are higher, specially when compared with currently desalination technologies^{11,49}. Therefore, both materials are capable of providing a high water permeability. The question is whether these materials are also able to effectively clean the water by removing the ions.

IV. ION REJECTION EFFICIENCY

The other important aspect for the cleaning of water is the membrane ability to separate water and ions. In this way, we investigate how the cation valence and the pore size affects the percentage rejected ions. In the Figure 4 we show the percentage of total ions rejected by the 2D nanopores as a function of the applied pressure for the three cations. The pores diameters are the same from the discussed in the previous section.

The ion rejection by the smallest pores, 0.17 and 0.26 nm for graphene and MoS₂, respectively, was 100% for all applied pressures and cation solutions. This is expected since the pore size is much smaller than the hydration radii of the cations. Therefore, is more energetically favorable for the cation to remain in the bulk solution instead of strip off the water and enter the pore⁵⁰. As the pore diameter increases this energetic penalty becomes smaller. As well, the valence plays a crucial role here, with the monovalent ions having a smaller penalty than divalent and trivalent cations. In this way, for the nanopores with diameter 0.37 nm and 0.46 nm for graphene and MoS₂, respectively, Na⁺ and Cl⁻ ions flow through the pore reducing the rejection efficiency for both materials, as we can see in the

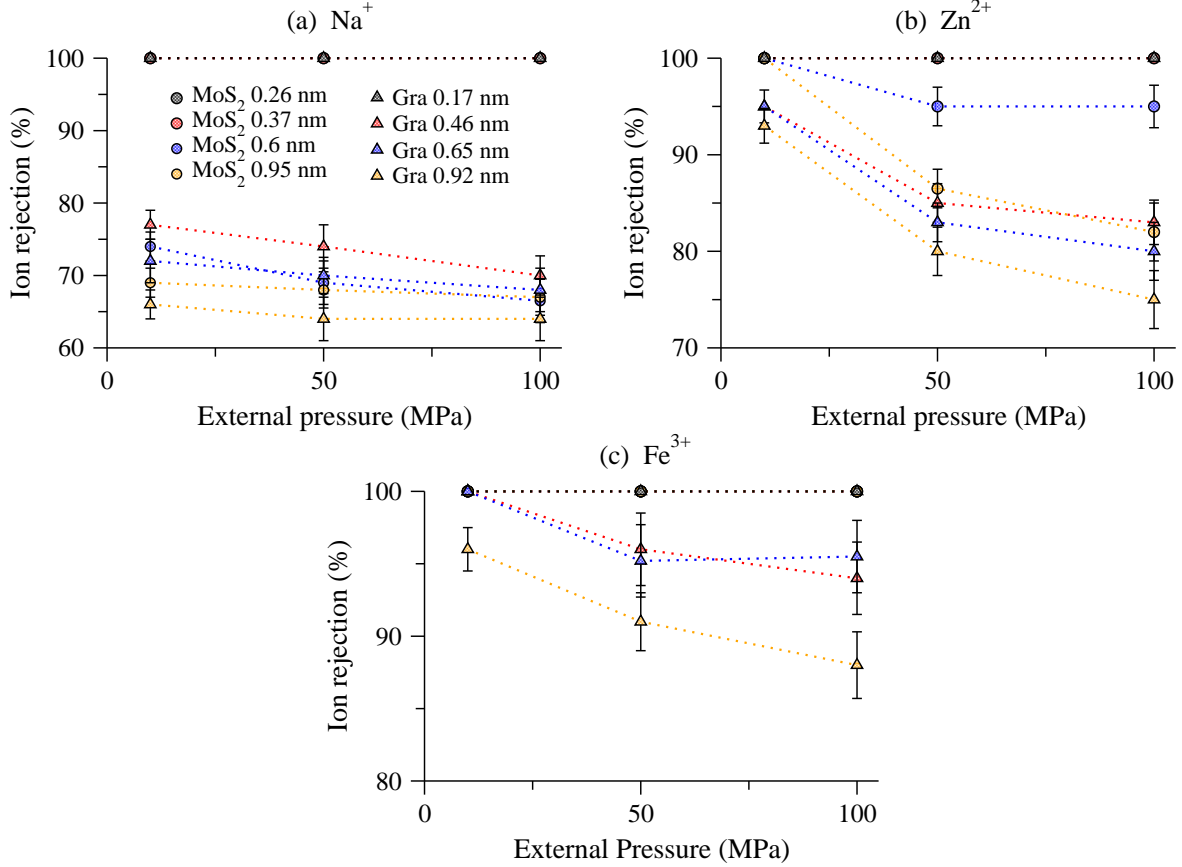


FIG. 4. Percentage of ion rejection by various pores as a function of the applied pressure. Pores with different diameters are considered.

Figure 4(a). However, it is important to note that the ion rejection performance of molybdenum disulfide membranes is superior from the observed for graphene membranes for all ranges of pressure, sizes and cation valences. For instance, for the divalent case Zn^{2+} , shown in the Figure 4(b) and the smaller ΔP the rejection is 100% for all pores sizes in the MoS₂ membrane, while for the graphene membrane we observe cation permeation for the bigger pores.

The MoS₂ membrane shows a very good performance for the rejection of the trivalent cation Fe^{3+} . As the Figure 4(c) shows, for all nanopore size and applied pressure the rejection is 100%. Such efficiency was not observed in the graphene membranes, were only the case with small pore diameter as 100% of iron rejection. Here, we should address that not only the hydration shell plays an important role in the cations rejection. While sodium chloride is uniformly dispersed in water and we do not observe clusters at the simulated concentration, the iron cations tend to form large clusters of ferric chlorides in solution, as

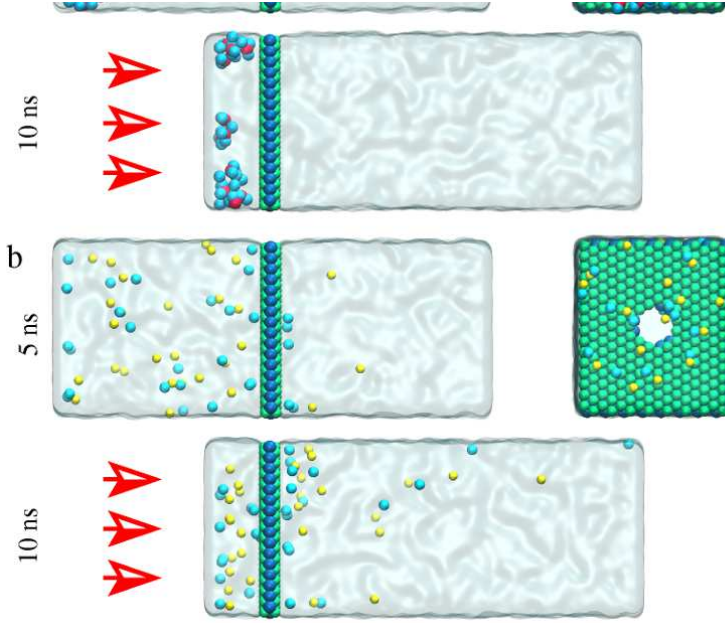


FIG. 5. Side and front view snapshots of (a) $\text{Fe}^{3+}\text{Cl}^{-}$ cluster formation preventing the ion passage through a 0.95 nm MoS_2 nanopore, and (b) monovalent $\text{Na}^{+}\text{Cl}^{-}$ passing through the same nanopore without clusterization for an external applied pressure of 50 MPa.

shown in Figure 5. Moreover, we observe this structures throughout the whole simulation and even at high pressure regime the clusters remains too large to overcome the pore. In fact, ferric chlorides are effective as primary coagulants due to their associative character in solution. At controlled concentrations, it is excellent for both drinking and wastewater treatment applications, including phosphorus removal⁵¹, sludge conditioning and struvite control^{52,53}. It also prevent odor and corrosion by controlling hydrogen sulfide formation. Additionally, our results indicates that the associative properties of ferric chlorides can be used to increase the efficiency of salt rejection by both MoS_2 and graphene nanopores, which may contribute in water cleaning devices.

V. SUMMARY AND CONCLUSIONS

We have calculated water fluxes through various MoS_2 and graphene nanopores and the respective percentage of total ions rejected by both materials as a function of the applied pressure gradient. Our results indicate that 2D nanoporous membranes are promising for water purification and salt rejection. The selectivity of the membranes was found to depend

on factors such as the pore diameter, the cationic valence and the applied pressure. Nevertheless, our results shows that the ion valency do not affect the water permeation – this is only affected by the pore size and chemical composition.

Particularly, our findings indicate that graphene is a better water conductor than MoS₂, with a higher permeability coefficient. Although, both material have presented high water fluxes. On the other hand, MoS₂ nanopores with water accessible pore diameters ranging from 0.26 to 0.95 nm strongly reject ions even at theoretically high pressures of 100 MPa. Additionally, the rejection is shown to depend strongly on the ion valence. It reaches 100% for trivalent ferric chloride (Fe³⁺Cl₃⁻) for all MoS₂ pore sizes and applied pressures. This is a direct result of the ability of heavy metals to form agglomerates, eventually exhibiting long ionic chains. At the same time, this did not affected the water flux. Then, the ferric chloride properties can be used to improve the effectiveness of 2D material based nanofilters. New studies are been performed in this direction.

ACKNOWLEDGMENTS

We thank the Brazilian agencies CNPq and INCT-FCx for the financial support, CENA-PAD/SP and CESUP/UFRGS for the computer time.

REFERENCES

- ¹D. Ko, J. S. Lee, H. A. Patel, M. H. Jakobsen, Y. Hwange, C. T. Yavuzan, H. B. Hansen, and H. R. Andersen, *J. Hazard. Mater.* **332**, 140 (2017).
- ²M. B. Gumpu, S. Sethuraman, U. M. Krishnan, and J. B. B. Rayappan, *Sens. Actuators B: Chem.* **213**, 515 (2015).
- ³M. Li, *Desalination* **422**, 124 (2017).
- ⁴L. Wang, M. S. H. Boutilier, P. R. Kidambi, D. Jang, N. G. Hadjiconstantinou, and R. Karnik, *Nat. Nanotech.* **12**, 509 (2017).
- ⁵K. Celebi, J. Buchheim, R. M. Wyss, A. Droudian, P. Gasser, I. Shorubalko, J.-I. Kye, C. Lee, and H. G. Park, *Science* **344**, 289 (2014).
- ⁶Q. Xu, H. Xu, J. Chen, Y. Lv, C. Dong, and T. S. Sreepasad, *Inorg. Chem. Front.* **2**, 417 (2015).

- ⁷K. C. Kemp, H. Seema, M. Saleh, N. H. Le, K. Mahesh, V. Chandra, and K. S. Kim, *Nanoscale* **5**, 3149 (2013).
- ⁸L. Huang, M. Zhang, C. Li, and G. Shi, *J. Phys. Chem. Lett.* **6**, 2806 (2015).
- ⁹J. Kou, J. Yao, L. Wu, X. Zhou, H. Lu, F. Wu, and J. Fan, *Phys. Chem. Chem. Phys.* **18**, 22210 (2016).
- ¹⁰W. Li, Y. Yang, J. K. Weber, G. Zhang, and R. Zhou, *ACS Nano* **10**, 1829 (2016).
- ¹¹M. Heiranian, A. B. Farimani, and N. R. Aluru, *Nat. Commun.* **6**, 8616 (2015).
- ¹²W. Lei, D. Portehault, D. Liu, S. Qin, and Y. Chen, *Nature Comm.* **4**, 1777 (2013).
- ¹³J. Azamat, B. S. Sattary, A. Khataee, and S. W. Joo, *J. Mol. Graph. Model.* **61**, 13 (2015).
- ¹⁴M. M. Pendergast and E. M. Hoek, *Energy Environ. Sci.* **4**, 1946 (2011).
- ¹⁵S. H. Jamali, T. J. H. Vlugt, and L.-C. Lin, *J. Phys. Chem. C* **121**, 11273 (2017).
- ¹⁶S. P. Surwade, S. N. Smirnov, I. V. Vlassioug, R. R. Unocic, G. M. Veith, S. Dai, and S. M. Mahurin, *Nat. Nanotech.* **10**, 459 (2015).
- ¹⁷D. Cohen-Tanugi and J. C. Grossman, *Nano Lett.* **12**, 3602 (2012).
- ¹⁸S. Garaj, W. Hubbard, A. Reina, J. Kong, D. Branton, and J. A. Golovchenko, *Nature* **467**, 190 (2010).
- ¹⁹K. Yoon, A. Rahnamoun, J. L. Swett, V. Iberi, D. A. Cullen, I. V. Vlassioug, A. Belianinov, S. Jesse, X. Sang, O. S. Ovchinnikova, A. J. Rondinone, R. R. Unocic, and A. C. van Duin, *ACS Nano* **10**, 8376 (2016).
- ²⁰S. C. OHern, D. Jang, S. Bose, J.-C. Idrobo, Y. Song, T. Laoui, J. Kong, and R. Karnik, *Nano Lett.* **15**, 3254 (2015).
- ²¹J. Feng, K. Liu, M. Graf, M. Lihter, R. D. Bulushev, D. Dumcenco, D. T. L. Alexander, D. Krasnozhan, T. Vuletic, A. Kis, and A. Radenovic, *Nano Lett.* **15**, 3431 (2015).
- ²²K. Liu, M. Lihter, A. Sarathy, S. Caneva, H. Qiu, D. Deiana, V. Tileli, D. T. L. Alexander, S. Hofmann, D. Dumcenco, A. Kis, J.-P. Leburton, and A. Radenovic, *Nano Lett.* **17**, 4223 (2017).
- ²³Z. Wang, Q. Tu, S. Zheng, J. J. Urban, S. Li, and B. Mi, *Nano Lett.* **17**, 7289 (2017).
- ²⁴D. Jang, J.-C. Idrobo, T. Laoui, and R. Karnik, *ACS Nano* **11**, 10042 (2017).
- ²⁵J. L. Achtyl, R. R. Unocic, L. Xu, Y. Cai, M. Raju, W. Zhang, R. L. Sacci, I. V. Vlassioug, P. F. Fulvio, P. Ganesh, D. J. Wesolowski, S. Dai, A. C. T. van Duin, M. Neurock, and F. M. Geiger, *Nature Communications* **6**, 6539 (2015).
- ²⁶G. Levita, P. Restuccia, and M. Righi, *Carbon* **107**, 878 (2016).

- ²⁷J. Abrahamand, K. S. Vasu, C. D. Williams, K. Gopinadhan, Y. Su, C. T. Cherian, J. Dix, E. Prestat, S. J. Haigh, I. V. Grigorieva, P. Carbone, A. K. Geim, and R. R. Nair, *Nat. Nanotech.* **12**, 546 (2017).
- ²⁸I. Moskowitz, M. A. Snyder, and J. Mittal, *J. Chem. Phys.* **141**, 18C532 (2014).
- ²⁹M. H. Köhler, J. R. Bordin, L. B. da Silva, and M. C. Barbosa, *Phys. Chem. Chem. Phys.* **19**, 12921 (2017).
- ³⁰J. R. Bordin and M. C. Barbosa, *Phys. A* **467**, 137 (2017).
- ³¹M. H. Köhler, R. C. Barbosa, L. B. da Silva, and M. C. Barbosa, *Phys. A* **468**, 733 (2017).
- ³²B. Corry, *J. Phys. Chem. B* **112**, 1427 (2008).
- ³³R. Das, M. E. Ali, S. B. A. Hamid, S. Ramakrishna, and Z. Z. Chowdhury, *Desalination* **336**, 97 (2014).
- ³⁴K. A. Mahmoud, B. Mansoor, A. Mansour, and M. Khraisheh, *Desalination* **356**, 208 (2015).
- ³⁵F. Fu and Q. Wang, *J. Environ. Management* **92**, 407 (2011).
- ³⁶S. Plimpton, *J. Comput. Phys.* **117**, 1 (1995).
- ³⁷J. Abascal and C. Vega, *J. Chem. Phys.* **123**, 234505 (2005).
- ³⁸J. P. Ryckaert, G. Ciccotti, and H. J. C. Berendsen, *J. Comput. Phys.* **23**, 327 (1977).
- ³⁹R. W. Hockney and J. W. Eastwood, *Computer Simulation Using Particles*, McGraw-Hill, New York, 1981.
- ⁴⁰A. Barati Farimani and N. R. Aluru, *J. Phys. Chem. B* **115**, 12145 (2011).
- ⁴¹T. Liang, S. R. Phillpot, and S. B. Sinnott, *Phys. Rev. B* **79**, 245110 (2009).
- ⁴²R. Fuentes-Azcatl and M. C. Barbosa, *J. Phys. Chem. B* **120**, 2460 (2016).
- ⁴³K. R. Hinkle, C. J. Jameson, and S. Murad, *J. Chem. Eng. Data* **61**, 1578 (2016).
- ⁴⁴S. Nosé, *Mol. Phys.* **52**, 255 (1984).
- ⁴⁵W. G. Hoover, *Phys. Rev. A* **31**, 1695 (1985).
- ⁴⁶J. R. Bordin, A. Diehl, and M. C. Barbosa, *J. Phys. Chem. B* **117**, 7047 (2013).
- ⁴⁷K. Falk, F. Sedlmeier, L. Joly, R. R. Netz, and L. Bocquet, *Nano Lett.* **10**, 4067 (2010).
- ⁴⁸G. Tocci, L. Joly, and A. Michaelides, *Nano Lett.* **14**, 6872 (2014).
- ⁴⁹J. Azamat and A. Khataee, *Comp. Mat. Sci.* **137**, 201 (2017).
- ⁵⁰J. R. Bordin, A. Diehl, M. C. Barbosa, and Y. Levin, *Phys. Rev. E* **85**, 031914 (2012).
- ⁵¹B. Kim, M. Gautier, P. Molle, P. Michel, and R. Gourdon, *Ecol. Eng.* **80**, 53 (2015).
- ⁵²O. Amuda and I. Amoo, *J. Hazard. Mater.* **141**, 778 (2007).

⁵³J. Sun, I. Pikaar, K. R. Sharma, J. Keller, and Z. Yuan, *Water Research* **71**, 150 (2015).